J Mol Model (2010) 16:677–691
DOI 10.1007/s00894-009-0580-4

ORIGINAL PAPER

CoMFA and CoMSIA analyses on 4-oxo-1,4-dihydroquinoline and 4-oxo-1,4-dihydro-1,5-, -1,6- and -1,8-naphthyridine derivatives as selective CB2 receptor agonists

Elena Cichero · Sara Cesarini · Luisa Mosti · Paola Fossa

Received: 25 May 2009 / Accepted: 24 July 2009 / Published online: 1 October 2009

Abstract Novel classes of CB2 agonists based on 4-oxo-1,4-dihydroquinoline and 4-oxo-1,4-dihydro-1,5-, -1,6- and -1,8-naphthyridine scaffolds have shown high binding affinity toward CB2 receptor and good selectivity over CB1. A computational study of comparative molecular fields analysis (CoMFA) and comparative molecular similarity indices analysis (CoMSIA) was performed, in order to identify the key structural features impacting their binding affinity. The final CoMSIA model resulted to be the more predictive, showing $r^2_{ncv} = 0.84$, $r^2_{cv} = 0.619$, SEE=0.369, and $r^2_{pred} = 0.75$. The study provides useful suggestions for the synthesis of new selective analogues with improved affinity.

Keywords Cannabinoid receptor · CB2 agonist · CoMFA · CoMSIA · 3D-QSAR

Introduction

Cannabinoid receptors interact with cannabinoid drugs including the classical cannabinoids, such as Δ^9- tetrahydrocannabinol (Δ^9-THC), their synthetic analogs and the endogenous cannabinoids [1–4]. The pharmacological effects of cannabinoids are mediated through at least two receptors, the cannabinoid 1 receptor (CB1) and the cannabinoid 2 receptor (CB2), even if at present there is some experimental evidence that supports the existence of additional types of cannabinoid receptors [5–7]. While CB1 is located principally in the central nervous system, CB2 is found in peripheral tissues, such as the spleen, tonsils and thymus. This subtype is of particular interest, since it has been identified as a potential target for therapeutic immune treatment, due to its involvement in signal transduction processes in the immune system. Furthermore, CB2 selective compounds were active in different neuropathic and inflammatory pain models [8–12]. Some neuroprotective roles have also been associated with CB2 agents, that could lead to the prevention of some neurodegenerative disorders, such as Huntington and Alzheimer's diseases [13–15]. Other studies have also highlighted potentials roles for CB2 in cancer [16, 17], multiple sclerosis [18] and bone regeneration [19, 20]. Since majority of CB2 receptor are distributed in peripheral tissues, with only low levels in neurons of central nervous system, centrally mediated side-effects would be greatly diminished with CB2 selective agents.

Both CB1 and CB2 belong to the large family of G-protein coupled receptors (GPCRs) [21] controlling a wide variety of signal transduction. Since GPCR are membrane proteins, their expression, purification, crystallization and structure determination present major challenges to the discovery of new drugs. In the absence of experimental data about human cannabinoid receptor 3D structures, computer-aided GPCR-targeted drug design can be performed on the basis of ligand-based modeling techniques, such as 3D-QSAR analysis or pharmacophore model generation.

Recently, novel classes of CB2 agonists based on 4-oxo-1,4-dihydroquinoline and 4-oxo-1,4-dihydro-1,5-, -1,6- and -1,8-naphthyridine scaffolds [22–25] (representative com-

E. Cichero (✉) · S. Cesarini · L. Mosti · P. Fossa
Dipartimento di Scienze Farmaceutiche,
Università degli Studi di Genova,
Viale Benedetto XV n.3,
16132 Genova, Italy
e-mail: cichero@unige.it

pounds **48**, **56**, **57** and **61** are depicted in Fig. 1) have shown high binding affinity toward CB2 receptor and good selectivity over the CB1 receptor.

In order to identify the key structural features impacting the binding affinity, and with the aim at providing useful suggestions for the design of new selective analogues with improved affinity, a computational study of comparative molecular fields analysis (CoMFA) and comparative molecular similarity indices analysis (CoMSIA) was performed.

Materials and methods

Data set

A dataset of 62 compounds showing the 4-oxo-1,4-dihydroquinoline and 4-oxo-1,4-dihydro-1,5-, -1,6- and -1,8-naphthyridine scaffolds (Table 1, compounds **1–62**), screened according to the same pharmacological protocol, were selected from literature [22–25]. All the compounds have been built, parameterized (Gasteiger-Huckel method) and energy minimized within MOE using MMFF94 forcefield [26].

3D-QSAR analysis

In the absence of crystallographic data about human CB2 3D structure, the ligand-based approach of CoMFA [27] and CoMSIA analyses [28], performed using Sybyl7.0 software [29], could provide a complementary tool for drug design. All compounds together were aligned on the basis of the common 1,3-disubstituted 4-oxo-1,4-dihydroquinoline or 4-oxo-1,4-dihydro-1,5-, -1,6- or -1,8-naphthyridine scaffold (in Fig. 1 the common scaffold is depicted in blue), by the align database command in Sybyl7.0, and CoMFA and CoMSIA models were calculated, with the aim of identifying the key structural features impacting the binding affinity.

Training set and test set

All the compounds were grouped into a training set, for model generation, and a test set, for model validation, containing 53 and 9 compounds respectively. The molecules of the test set represent 17% (estimated as a good percentage to validate a molecular model) of the training set. Both the training and the test set were divided manually according to a representative range of biological activities and structural variations. For QSAR analysis, K_i values have been transformed into pK_i values and then used as response variables. Compounds CB2 affinity covered 4 log orders.

CoMFA and CoMSIA interaction energies

CoMFA method [27] is a widely used 3D-QSAR technique to relate the biological activity of a series of molecules to their steric and electrostatic fields, which are calculated placing the aligned molecules, one by one, into a 3D cubic lattice with a 2 Å grid spacing. The van der Waals potential and Coulombic terms, which represent steric and electrostatic fields, respectively, were calculated using the standard Tripos force field method. The column-filtering threshold value was set to 2.0 kcal mol^{-1} to improve the signal-noise ratio. A methyl probe with a +1 charge was used to calculate the CoMFA steric and electrostatic fields. A 30 kcal mol^{-1} energy cut-off was applied to avoid infinity of energy values inside the molecule. The CoMSIA method [28] calculates five descriptors, namely steric, electrostatic and hydrophobic parameters, and H-bond donor and H-bond acceptor properties. The similarity index descriptors were calculated using the same lattice box employed for the CoMFA calculations and a sp^3 carbon as probe atom with a +1 charge, +1 hydrophobicity and +1 H-bond acceptor and +1 H-bond donor properties.

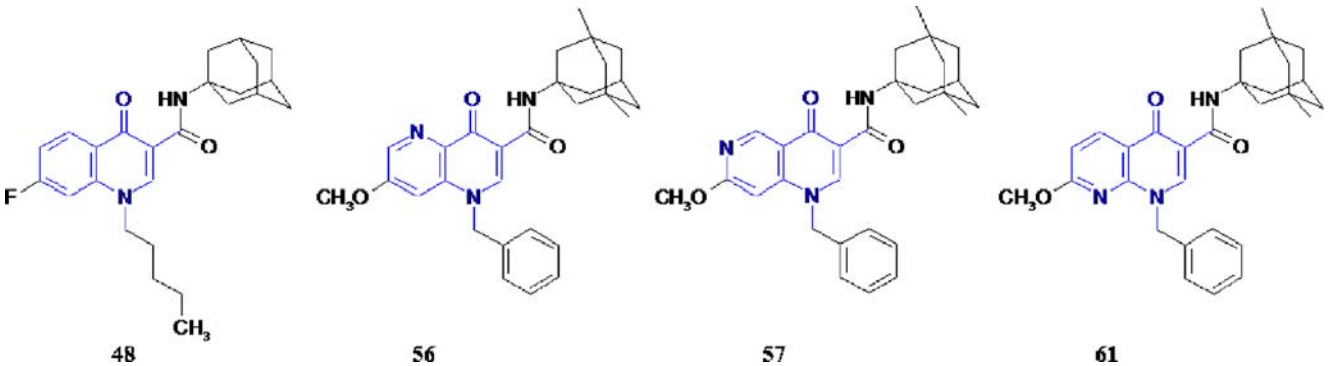

Fig. 1 Chemical structure of **48**, **56**, **57** and **61** as representatives of the 4-oxo-1,4-dihydroquinoline and 4-oxo-1,4-dihydro-1,5-, -1,6- and -1,8-naphthyridine derivatives, respectively. The common 1,3-disubstituted 4-oxo-1,4-dihydroquinoline or 4-oxo-1,4-dihydro-1,5-, -1,6- or -1,8-naphthyridine scaffold is depicted in blue

Table 1 Molecular structure of selective CB2 agonists **1**–**62**

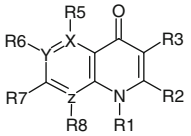

Comp.	R1	R2	R3	R5	R6	R7	R8	X	Y	Z
1	-$(CH_2)_4CH_3$	H	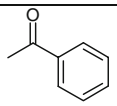	H	H	H	H	C	C	C
2	-$(CH_2)_4CH_3$	H	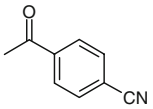	H	H	H	H	C	C	C
3	-$(CH_2)_4CH_3$	H	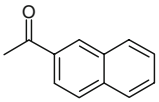	H	H	H	H	C	C	C
4	-$(CH_2)_3CH_3$	H	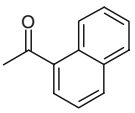	H	H	H	H	C	C	C
5	-$(CH_2)_4CH_3$	H	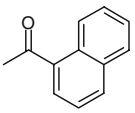	H	H	H	H	C	C	C
6	-$(CH_2)_5CH_3$	H	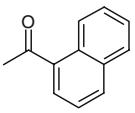	H	H	H	H	C	C	C
7	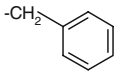	H	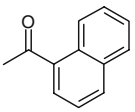	H	H	H	H	C	C	C
8	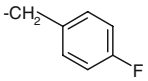	H	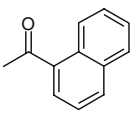	H	H	H	H	C	C	C
9	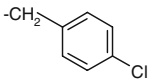	H	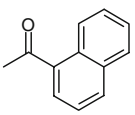	H	H	H	H	C	C	C
10	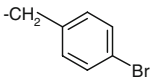	H	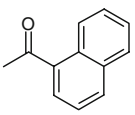	H	H	H	H	C	C	C
11	-$(CH_2)_3CH_3$	H	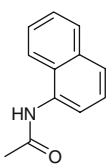	H	H	H	H	C	C	C

Partial least square (PLS) analysis and models validation

The partial least-squares (PLS) approach, an extension of the multiple regression analysis, was used to derive the 3D-QSAR models. CoMFA and CoMSIA descriptors were used as independent variables and pKi values were used as dependent variables. Prior to the PLS analysis, CoMFA and CoMSIA columns with a variance of less than 2.0 kcal mol^{-1} were

Table 1 (continued)

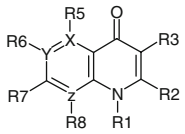

Comp.	R1	R2	R3	R5	R6	R7	R8	X	Y	Z
12	-$(CH_2)_4CH_3$	H	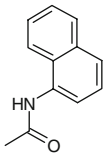	H	H	H	H	C	C	C
13	-$(CH_2)_5CH_3$	H	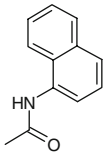	H	H	H	H	C	C	C
14	-$(CH_2)_4CH_3$	H	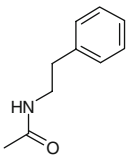	H	H	H	H	C	C	C
15	-$(CH_2)_4CH_3$	H	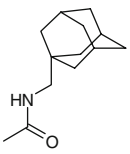	H	H	H	H	C	C	C
16		H	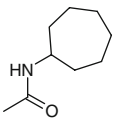	H	H	H	H	C	C	C
17	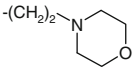	H	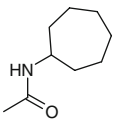	H	H	H	H	C	C	C
18	-$(CH_2)_4CH_3$	H	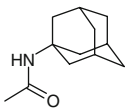	H	H	H	H	C	C	C
19	-$(CH_2)_4CH_3$	H	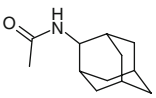	H	H	H	H	C	C	C
20	-$(CH_2)_4CH_3$	H	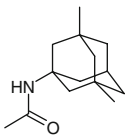	H	H	H	H	C	C	C
21		H	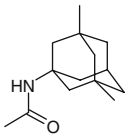	H	H	H	H	C	C	C

Table 1 (continued)

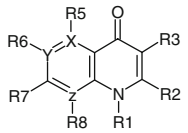

Comp.	R1	R2	R3	R5	R6	R7	R8	X	Y	Z
22	-$(CH_2)_4CH_3$	CH_3	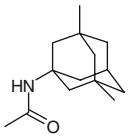	H	H	H	H	C	C	C
23	-$(CH_2)_4CH_3$		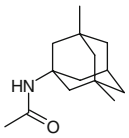	H	H	H	H	C	C	C
24	-$(CH_2)_4CH_3$		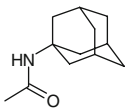	H	H	H	H	C	C	C
25	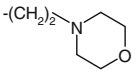	H	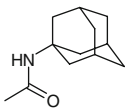	H	H	H	H	C	C	C
26	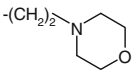	H	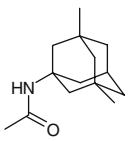	H	H	H	H	C	C	C
27	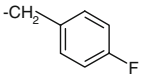	H	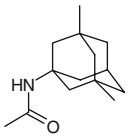	H	H	H	H	C	C	C
28	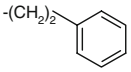	H	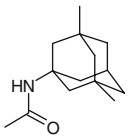	H	H	H	H	C	C	C
29	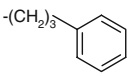	H	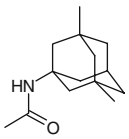	H	H	H	H	C	C	C
30	-$(CH_2)_4CH_3$	H	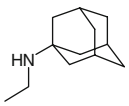	H	H	H	H	C	C	C
31	-$(CH_2)_4CH_3$	H	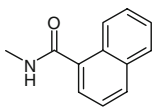	H	H	H	H	C	C	C
32	-$(CH_2)_4CH_3$	H	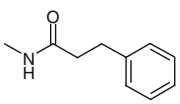	H	H	H	H	C	C	C

Table 1 (continued)

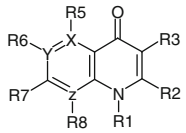

Comp.	R1	R2	R3	R5	R6	R7	R8	X	Y	Z
33	-$(CH_2)_4CH_3$	H	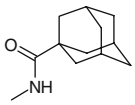	H	H	H	H	C	C	C
34	-$(CH_2)_4CH_3$	H	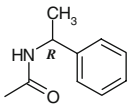	H	H	F	H	C	C	C
35	-$(CH_2)_4CH_3$	H	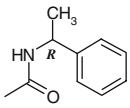	H	H		H	C	C	C
36	-$(CH_2)_4CH_3$	H	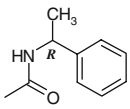	H	H	OCH_2CH_3	H	C	C	C
37	-$(CH_2)_4CH_3$	H	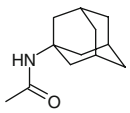	H	H	Cl	CH_3	C	C	C
38	-$(CH_2)_4CH_3$	H	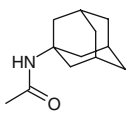	H	CF_3	H	H	C	C	C
39	-$(CH_2)_4CH_3$	H	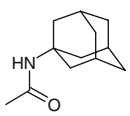	H	-$CH(CH_3)_2$	H	H	C	C	
40	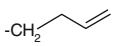	H	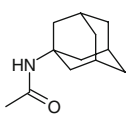	H	Br	H	H	C	C	
41	-$(CH_2)_4CH_3$	H	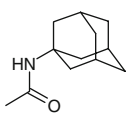	H	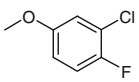	H	H	C	C	
42	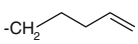	H	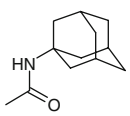	H	Br	H	H	C	C	
43	-$(CH_2)_4CH_3$	H	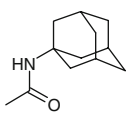	H	Br	H	H	C	C	
44	-$(CH_2)_4CH_3$	H	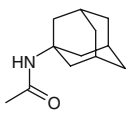	H	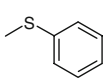	H	H	C	C	

filtered by using column filtering to improve the signal-to-noise ratio.

The leave one out (LOO) cross-validation method was used to check the predictivity of the derived model and to identify the optimal number of components (ONC) leading to the highest cross-validated r^2 $\left(r^2_{cv}\right)$. In the LOO methodology, one molecule is omitted from the dataset and a model is derived involving the rest of the compounds.

Table 1 (continued)

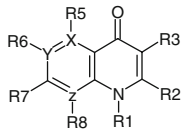

Comp.	R1	R2	R3	R5	R6	R7	R8	X	Y	Z
45	-$(CH_2)_4CH_3$	H	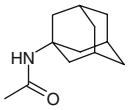		H	H		C	C	C
46	-CH_2 	H	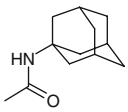		H	H		C	C	C
47	-$(CH_2)_4CH_3$	H	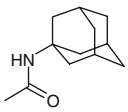	H	F		H	C	C	C
48	-$(CH_2)_4CH_3$	H	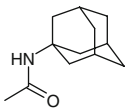	H	H	F	H	C	C	C
49	-$(CH_2)_4CH_3$	H	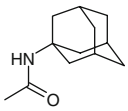	H	H	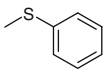	H	C	C	C
50	-$(CH_2)_4CH_3$	H	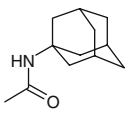	H	H	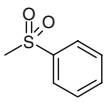	H	C	C	C
51	-$(CH_2)_4CH_3$	H	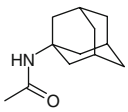	H	H	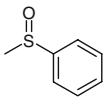	H	C	C	C
52	-$(CH_2)_4CH_3$	H	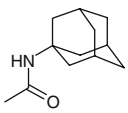	H		H	H	C	C	C
53	-$(CH_2)_4CH_3$	H	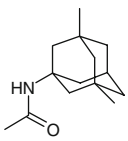	H	Cl	H	H	C	C	C
54	-$(CH_2)_4CH_3$	H	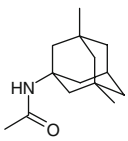	H	H	Cl	H	C	C	C

Employing this model, the activity of the omitted molecule is then predicted.

The ONC obtained from cross-validation methodology was used in the subsequent regression model. Final CoMFA and CoMSIA models were generated using non-cross-validated PLS analysis. To further assess the statistical confidence and robustness of the derived models, a 100-cycle bootstrap analysis was performed. This is a procedure in which n random selections out of the original set of n objects are performed several times (100-times were required to obtain a good statistical information). In each run, some objects may not be included in the PLS analysis, whereas some others might be included more than once. The mean correlation coefficient is represented as bootstrap $r^2\left(r^2_{boot}\right)$.

Table 1 (continued)

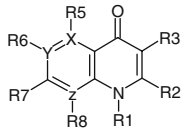

Comp.	R1	R2	R3	R5	R6	R7	R8	X	Y	Z
55	-$(CH_2)_4CH_3$	H	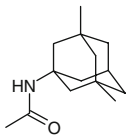	H	H	H	Cl	C	C	C
56	-$(CH_2)_4CH_3$	H	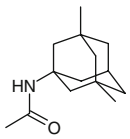	H	H	H	H	N	C	C
57	-$(CH_2)_4CH_3$	H	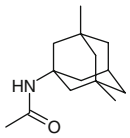	H	H	H	H	C	N	C
58	-$(CH_2)_4CH_3$	H	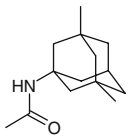	H	H	H	H	C	C	N
59		H	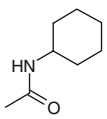	H	H	-O-CH_3	H	C	C	C
60	-$(CH_2)_2$- 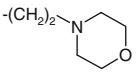	H	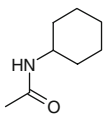	H	H	-O-CH_3	H	C	C	C
61		H	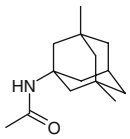	H	H	-O-CH_3	H	C	C	N
62	-$(CH_2)_2$- 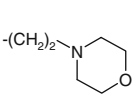	H	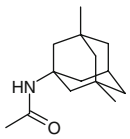	H	H	-$N(CH_3)_2$	H	C	C	N

Predictive correlation coefficient $\left(r^2_{pred}\right)$

To further validate the CoMFA and CoMSIA derived model, the predictive ability for the test set of compounds (expressed as r^2_{pred}) was determined by using the following equation:

$$r^2_{pred} = (SD - PRESS)/SD,$$

SD is the sum of the squared deviations between the biological activities of the test set molecules and the mean activity of the training set compounds and PRESS is the sum of the squared deviation between the observed and the predicted activities of the test set compounds.

All calculations were carried out using a PC running the Windows XP operating system and an SGI O2 Silicon Graphics.

Results and discussion

CoMFA and CoMSIA analyses

To develop the 3D-QSAR analyses, **1–62** were aligned (Fig. 2) on the basis of the common 1,3-disubstituted 4-oxo-1,4-dihydroquinoline or 4-oxo-1,4-dihydro-1,5-, -1,6-

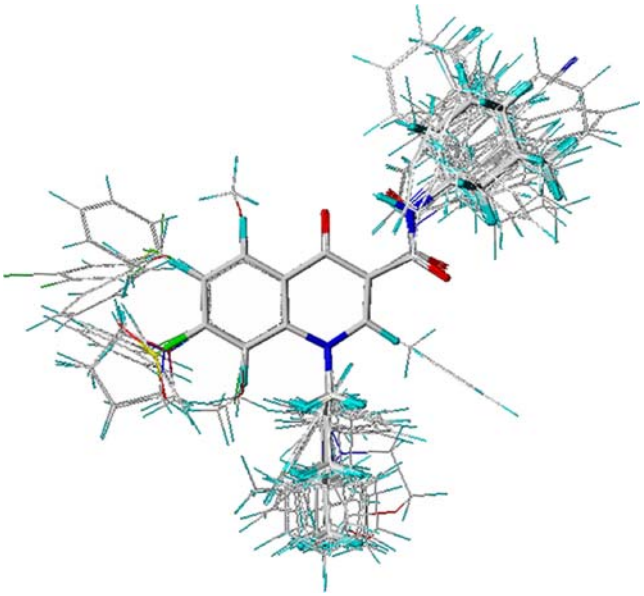

Fig. 2 Alignment of **1**–**62** employed for CoMFA and CoMSIA analyses

or -1,8-naphthyridine scaffold (in Fig. 1 the common scaffold is depicted in blue).

CoMFA and CoMSIA analyses were performed dividing compounds **1–62** into a training set (**1**, **2**, **4**, **5**, **7**–**10**, **12**–**21**, **23**–**27**, **29**–**34**, **36**–**51**, **53**, **55**–**57**, **59**–**62**) for model generation and into a test set (**3**, **6**, **11**, **22, 28**, **35**, **52**, **54**, **58**) for model validation. CoMFA and CoMSIA studies were developed using, respectively, CoMFA steric and electrostatic fields and CoMSIA steric, electrostatic, hydrophobic, H-bond acceptor, and H-bond donor properties, as independent variables, and the ligand pKi as dependent variable.

The final CoMFA model was generated employing non-cross-validated PLS analysis with the optimum number of components (ONC=5) to give a non-cross validated $r^2\left(r^2_{ncv}\right) = 0.90$, a test set $r^2\left(r^2_{pred}\right) = 0.71$, standard error of estimate (SEE) = 0.279, steric contribution = 0.437 and electrostatic contribution = 0.563. The model reliability thus generated was supported by bootstrapping results. All statistical parameters supporting CoMFA model are reported in Table 2.

A CoMSIA model consisting of steric, electrostatic, hydrophobic, H-bond acceptor, and H-bond donor fields with a $r^2_{ncv} = 0.84$, a $r^2_{pred} = 0.75$, SEE=0.369, steric contribution = 0.177, electrostatic contribution = 0.200, hydrophobic contribution = 0.310, H-bond acceptor contribution = 0.163, and H-bond donor contribution = 0.150 was derived. All statistical parameters supporting CoMSIA model are reported in Table 3.

Experimental and predicted binding affinities values for the training set and test set are reported in Table 4, while distribution of experimental and predicted pK_i values for training set and test set according to CoMFA and CoMSIA models are represented in Fig. 3.

Table 2 Summary of CoMFA results

No. compounds	53
Optimal number of components (ONC)	5
Leave one out r^2 $\left(r^2_{loo}\right)$	0.544
Cross-validated r^2 $\left(r^2_{cv}\right)$	0.635
Std. error of estimate (SEE)	0.279
Non cross-validated r^2 $\left(r^2_{ncv}\right)$	0.90
F value	93.822
Steric contribution	0.437
Electrostatic contribution	0.563
Bootstrap r^2 $\left(r^2_{boot}\right)$	0.94
Standard error of estimate $r^2_{boot}\left(SEE\ r^2_{boot}\right)$	0.230
Test set r^2 $\left(r^2_{pred}\right)$	0.71

As shown in Fig. 4 (for simplicity, only the structure of compound **48**, showing the highest pK_i value in the dataset, is depicted and used as reference), the steric contour map predicts disfavored interaction polyhedra (yellow) around position 2 and in the vicinity of position 7 of the scaffold, and near the methyl group of the R1 *n*-pentyl. The R3 adamantyl group is occupied by a green region (favored) partially surrounded by yellow polyhedra. The reliability of the steric map calculations is verified by the higher affinity of **18** (R2 = H, pK_i=7.79) compared to that of **24** (R2 = phenyl, pK_i=6.47), and the higher pK_i value of **20** (R2 = H, pK_i=7.80) in comparison with that of **22** (R2 = methyl, pK_i=6.70) and **23** (R2 = phenyl, pK_i=6.92). Moreover, the CoMFA steric map is in agreement with the following affinity trends: *i*) compounds

Table 3 Summary of CoMSIA results

No. compounds	53
Optimal number of components (ONC)	4
Leave one out r^2 $\left(r^2_{loo}\right)$	0.521
Cross-validated r^2 $\left(r^2_{cv}\right)$	0.619
Std. error of estimate (SEE)	0.369
Non cross-validated r^2 $\left(r^2_{ncv}\right)$	0.84
F value	41.551
Steric contribution	0.177
Electrostatic contribution	0.200
Hydrophobic contribution	0.310
H-bond acceptor contribution	0.163
H-bond donor contribution	0.150
Bootstrap r^2 $\left(r^2_{boot}\right)$	0.93
Standard error of estimate $r^2_{boot}\left(SEE\ r^2_{boot}\right)$	0.231
Test set r^2 $\left(r^2_{pred}\right)$	0.75

Table 4 Experimental and predicted pK_i values of compounds **1–62** according 3D-QSAR analyses

Compound		CoMFA model		CoMSIA model	
	Exp. pK_i	Pred. pK_i	Residual	Pred. pK_i	Residual
1	6.35	6.35	0.00	6.43	−0.08
2	6.11	6.34	−0.23	6.00	0.11
3[a]	5.89	6.84	−0.95	6.37	−0.48
4	5.81	6.04	−0.23	6.42	−0.61
5	6.81	6.59	0.23	6.43	0.38
6[a]	6.24	6.31	−0.07	6.33	−0.09
7	6.18	6.18	0.00	6.31	−0.13
8	6.65	6.27	0.38	6.27	0.38
9	5.95	6.10	−0.15	6.18	−0.23
10	6.02	6.03	−0.01	6.10	−0.08
11[a]	6.34	5.81	0.53	6.03	0.31
12	6.43	6.45	−0.02	6.04	0.39
13	6.07	6.20	−0.13	5.96	0.11
14	6.70	6.65	0.05	6.71	−0.01
15	7.30	7.71	−0.41	7.34	−0.04
16	8.19	7.44	0.75	7.18	1.01
17	7.55	7.83	−0.28	7.50	0.05
18	7.79	7.75	0.04	7.68	0.11
19	7.87	7.88	−0.01	7.46	0.41
20	7.80	7.28	0.52	7.34	0.46
21	6.18	7.07	−0.89	7.25	−1.07
22[a]	6.70	6.73	−0.03	7.07	−0.37
23	6.92	6.65	0.27	6.45	0.47
24	6.47	6.75	−0.28	6.78	−0.31
25	6.82	6.85	−0.03	7.23	−0.40
26	6.66	6.37	0.29	6.88	−0.22
27	7.08	6.94	0.14	7.17	−0.09
28[a]	6.48	7.28	−0.80	7.43	−0.95
29	6.80	6.63	0.17	6.97	−0.17
30	5.78	5.58	0.20	5.55	0.23
31	6.58	6.58	0.00	6.65	−0.07
32	5.95	6.17	−0.22	6.28	−0.33
33	7.59	7.23	0.36	7.23	0.36
34	7.97	8.17	−0.20	8.08	−0.11
35[a]	7.77	7.67	0.10	7.88	−0.11
36	7.62	7.50	0.12	7.84	−0.22
37	7.59	7.74	−0.15	8.05	−0.46
38	7.94	8.07	−0.13	8.21	−0.27
39	8.20	8.20	0.00	7.97	0.23
40	7.62	7.65	−0.03	7.84	−0.22
41	7.79	7.75	0.04	7.86	−0.07
42	8.03	8.17	−0.14	7.87	0.16
43	7.84	7.83	0.01	7.84	0.00
44	8.47	8.38	0.09	8.50	−0.03
45	7.28	7.83	−0.55	7.68	−0.40
46	8.04	7.86	0.18	7.74	0.30
47	8.44	8.29	0.15	8.60	−0.16

Table 4 (continued)

Compound		CoMFA model		CoMSIA model	
	Exp. pK_i	Pred. pK_i	Residual	Pred. pK_i	Residual
48	9.10	8.51	0.59	8.20	0.90
49	8.80	8.77	0.03	8.60	0.20
50	9.05	9.13	−0.07	8.92	0.13
51	8.46	8.48	−0.02	8.42	0.04
52[a]	8.42	8.09	0.33	7.99	0.44
53	7.26	7.42	−0.16	7.48	−0.22
54[a]	8.28	7.84	0.44	7.75	0.53
55	7.56	7.24	0.32	7.47	0.09
56	6.59	6.82	−0.23	6.72	−0.13
57	7.51	7.53	−0.02	7.16	0.35
58[a]	7.63	7.74	−0.11	7.48	0.15
59	7.10	7.27	−0.17	7.40	−0.30
60	7.10	7.29	−0.19	7.53	−0.43
61	7.96	7.91	0.05	7.81	0.15
62	7.03	6.88	0.15	7.25	−0.22

a Test set compounds

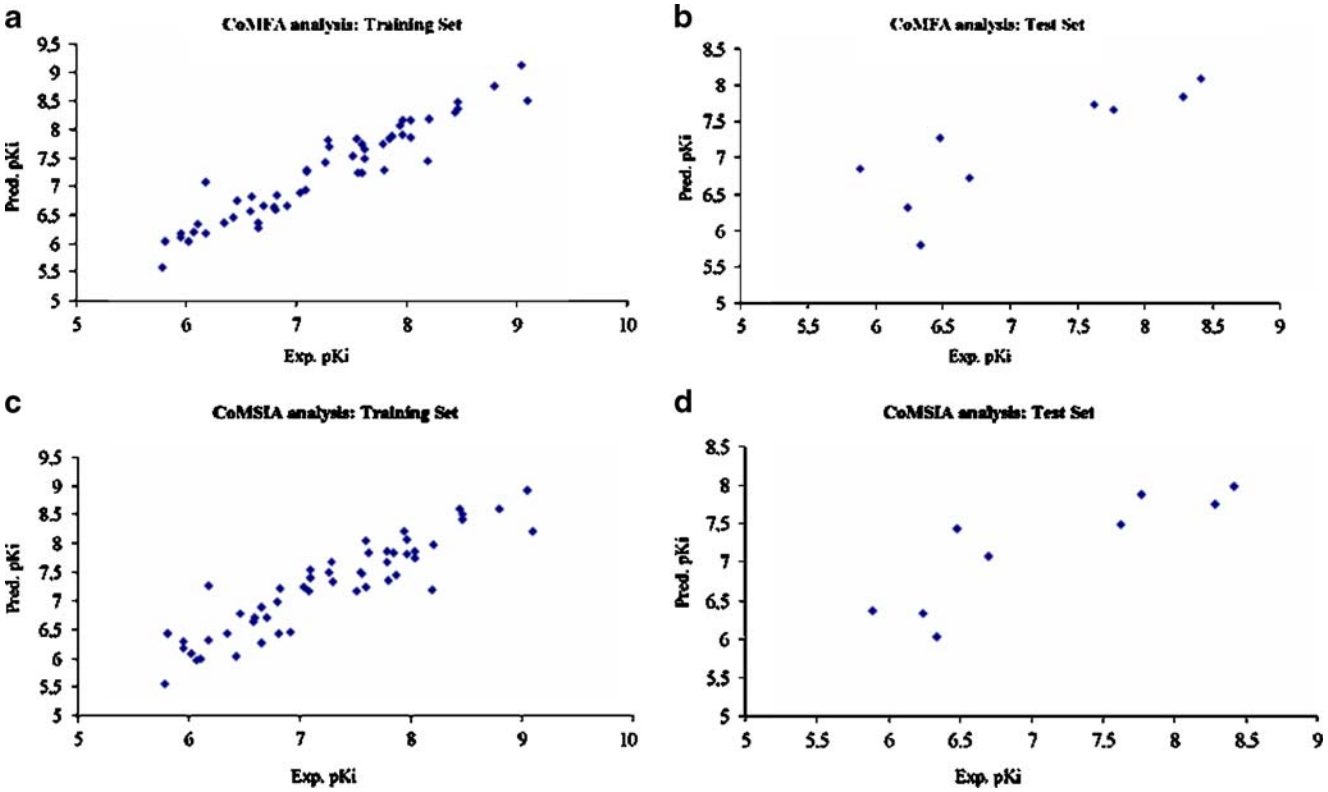

Fig. 3 Distribution of experimental and predicted pK_i values for training set compounds according to CoMFA analysis (**a**), for test set compounds according to CoMFA analysis (**b**), for training set compounds according to CoMSIA analysis (**c**), and for test set compounds according to CoMSIA analysis (**d**)

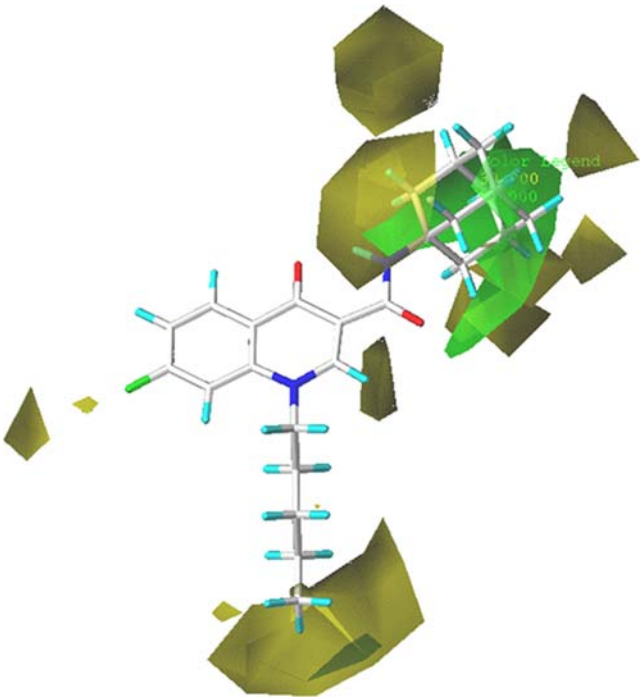

Fig. 4 Contour maps of CoMFA steric regions (green, favored; yellow, disfavored) are depicted around compound **48**, shown in stick mode and colored by atom type

18, **19**, **20** and **33** (pK_i=7.59–7.87) > **15** (pK_i=7.30) > **12**, **14**, **31** and **32** (pK_i=5.95–6.70) {*i.e.* R3=CONH-(1- or 2-adamantyl), CONH-[1-(3,5-dimethyladamantyl)] and NHCO-(1-adamantyl) > CONH-(1-adamantylmethyl) > CONH-(1-naphthyl), CONH-(2-phenylethyl), NHCO-(1-naphthyl) and NHCO-(2-phenylethyl)}; *ii*) compound **16** (pK_i=8.19) > **21** (pK_i=6.18), and analogue **17** (pK_i=7.55) > **25** (pK_i=6.82) and **26** (pK_i=6.66) {*i.e.* R3 = CONH-cycloheptyl > CONH-(1-adamantyl) and CONH-[1-(3,5-dimethyladamantyl)]}; *iii*) **1** (pK_i=6.35) > **3** (pK_i=5.89) (*i.e.*, R3 = benzoyl > 2-naphthoyl).

The reliability of the steric map calculations is verified also by the higher pK_i value of **34** (R7 = F, pK_i=7.97) compared to that of **35** (R7 = 1-pyrrolidinyl, pK_i=7.77) and **36** (R7 = ethoxy, pK_i=7.62), and by the following affinity trends: *i*) compound **12** (pK_i=6.43) > **13** (pK_i=6.07), and analogue **5** (pK_i = 6.81) > **6**, **7** and **8** (pK_i=6.18–6.65) > **9** (pK_i=5.95) and **10** (pK_i=6.02) (*i.e.*, R1 = *n*-pentyl > *n*-hexyl, benzyl and 4-fluorobenzyl > 4-chloro- and 4-bromobenzyl); *ii*) **20** (pK_i=7.80) > **27** (pK_i=7.08) > **28** (pK_i=6.48) and **29** (pK_i=6.80) (*i.e.*, R1 = *n*-pentyl > 4-fluorobenzyl > 2-phenylethyl and 3-phenylpropyl).

According to the electrostatic field contour map of the CoMFA analysis plotted in Fig. 5, less positive moieties are predicted to be favored (red areas) in proximity of scaffold position 7 and around the adamantyl position 2, the carbonyl oxygen atom and the methyl group of the *n*-pentyl. On the other hand, more electropositive substituents are predicted to be beneficial (blue areas) around the scaffold position 7 and the adamantyl position 8. Moreover, a blue region is located between the adamantyl positions 1 and 6. Accordingly, compounds **8** (pK_i=6.65), **27** (pK_i= 7.08) and **42** (pK_i=8.03) show higher pK_i values than the corresponding derivatives **7** (pK_i=6.18), **21** (pK_i=6.18) and **43** (pK_i=7.84), respectively (*i.e.* R1 = 4-fluorobenzyl > benzyl and R1 = pent-1-en-5-yl > *n*-pentyl). Besides, the results are in agreement with the following affinity trends: *i*) **18** (pK_i=7.79) > **33** (pK_i=7.59) > **30** (pK_i=5.78) [*i.e.*, R3 = CONH-(1-adamantyl) > NHCO-(1-adamantyl) > CH_2NH-(1-adamantyl)]; *ii*) **14** (pK_i=6.70) > **32** (pK_i=5.95) [*i.e.*, R3 = CONH-(2-phenylethyl > NHCO-(2-phenylethyl)]; *iii*) **1** (pK_i=6.35) > **2** (pK_i=6.11) (*i.e.*, R3 = benzoyl > 4-cyanobenzoyl).

The reliability of the electrostatic map calculations is verified also by the very high binding affinity of **48** (R7 = fluoro, pK_i=9.10), **49** (R7 = S-phenyl, pK_i=8.80), **50** (R7= SO_2-phenyl, pK_i=9.05) and **51** (R7=SO-phenyl, pK_i=8.46) compared to that of **18** (R7 = H, pK_i=7.79), by the higher pK_i values of **54** (R7 = chloro, pK_i=8.28) in comparison with that of **20** (R7 = H, pK_i=7.80), and by the high binding affinity of **34** (R7 = fluoro, pK_i=7.97), **35** (R7 = 1-pyrrolidinyl, pK_i=7.77) and **36** (R7 = ethoxy, pK_i=7.62).

The CoMSIA steric and electrostatic regions are in agreement with the CoMFA steric and electrostatic areas.

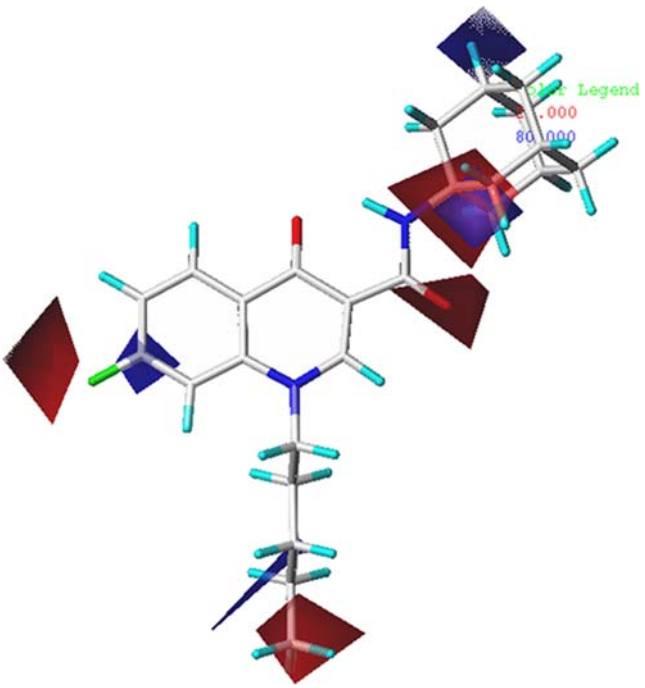

Fig. 5 Contour maps of CoMFA electrostatic regions are shown around compounds **48**. Blue regions are favorable for more positively charged groups; red regions are favorable for less positively charged groups

The calculated CoMSIA hydrophobic map (Fig. 6) displays yellow areas (favored) around the scaffold position 7, in proximity of the region between positions 6 and 7, and near position 2. In addition, yellow polyhedra surround the adamantyl moiety and enclose the methylenes of the *n*-pentyl group. The methyl of the *n*-pentyl group is enclosed by an uncolored area, in its turn surrounded by yellow polyhedra.

Accordingly, the R1 *n*-pentyl derivatives **18** (pK_i=7.79) and **20** (pK_i=7.80) shown higher pK_i values than the corresponding R1 *N*-morpholinethyl analogues **25** (pK_i=6.82) and **26** (pK_i=6.66). The results are also in agreement with the higher binding affinity of **20** (Y = C, pK_i=7.80) in comparison with that of **57** (Y = N, pK_i=7.51), and with the higher pK_i values of **38** (R6 = trifluoromethyl, pK_i=7.94), **39** (R6 = *i*-propyl, pK_i=8.20), **43** (R6 = bromo, pK_i=7.84), **44** (R6 = S-phenyl, pK_i=8.47), **52** (R6 = phenyl, pK_i=8.42) and **47** (R6 = fluoro, R7 = 1-pyrrolyl, pK_i=8.44) compared to that of **18** (R6 = H, pK_i=7.79). In addition, the reliability of the hydrophobic map calculations is verified by the very high binding affinity of **48** (R7 = fluoro, pK_i=9.10), **49** (R7 = S-phenyl, pK_i=8.80), **50** (R7 = SO_2-phenyl, pK_i=9.05) and **51** (R7 = SO-phenyl, pK_i=8.46) compared to that of **18** (R7 = H, pK_i=7.79), by the higher pK_i values of **54** (R7 = chloro, pK_i=8.28) in comparison with that of **20** (R7 = H, pK_i=7.80), and by the high binding affinity of **34** (R7 = fluoro, pK_i=7.97), **35** (R7 = 1-pyrrolidinyl, pK_i=7.77) and **36** (R7 = ethoxy, pK_i=7.62). Moreover, in accordance with the CoMFA hydrophobic map, **18** [R3 = CONH-(1-adamantyl)], **19** [R3 = CONH-(2-adamantyl)] and **20** {R3 = CONH-[1-(3,5-dimethyladamantyl)]} (pK_i=7.79–7.87) result to be more potent than **14** [R3 = CONH-(2-phenylethyl), pK_i=6.70], and **33** [R3 = NHCO-(1-adamantyl), pK_i=7.59] is more potent than **32** [R3 = NHCO-(2-phenylethyl), pK_i=5.95].

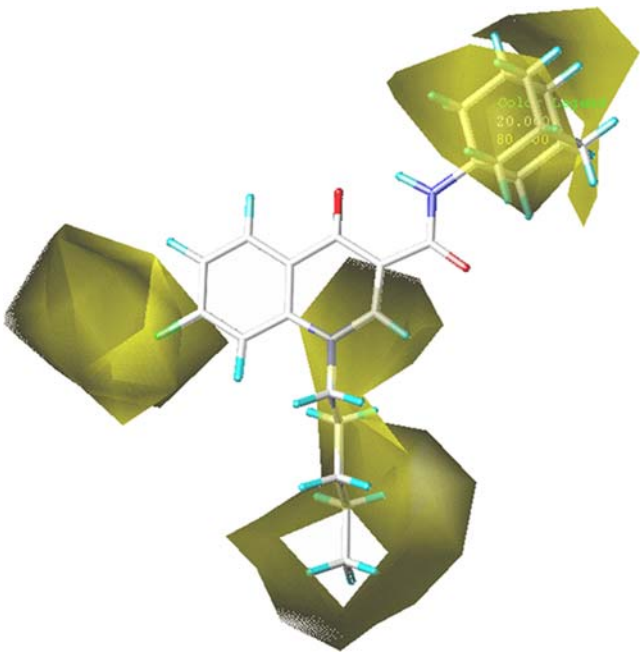

Fig. 6 Contour maps of CoMSIA hydrophobic regions (yellow, favored; white, disfavored) are depicted around compounds **48**, shown in stick mode and colored by atom type

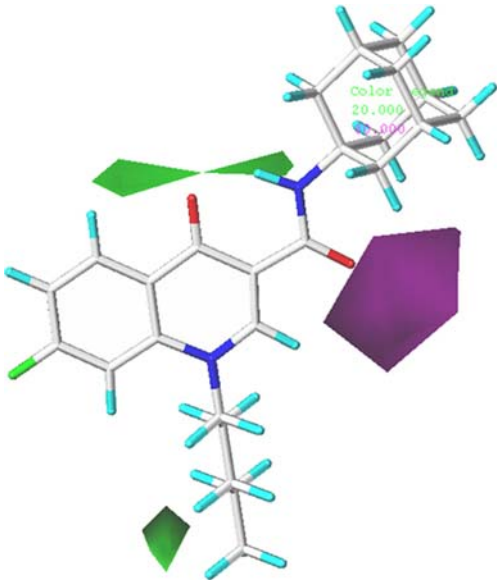

Fig. 7 CoMSIA hydrogen bond acceptor polihedra are shown around compounds **48** depicted in stick mode and colored by atom type. H-bond acceptor groups: magenta, favored; green, disfavored

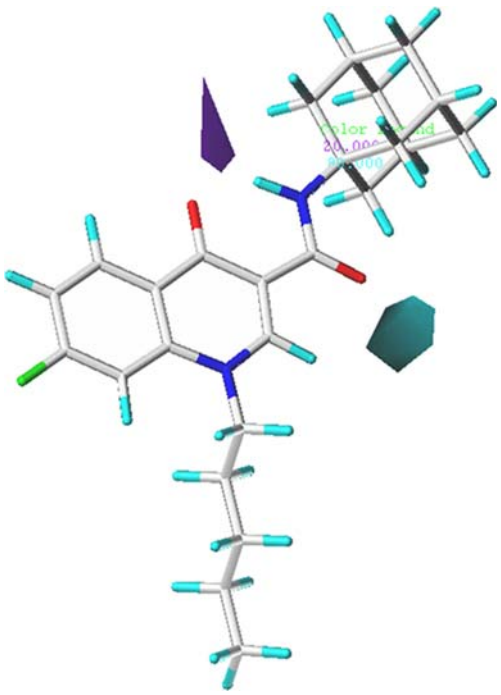

Fig. 8 CoMSIA hydrogen bond donor polihedra are shown around compounds **48** depicted in stick mode and colored by atom type. H-bond donor groups: purple, favored; cyan, disfavored

The calculated CoMSIA H-bond acceptor map (Fig. 7) displays a magenta area (favored) in proximity of the oxygen atom of the R3 amidic group, and green polyhedra (unfavorable) near the nitrogen atom of the R3 amidic function, and in the vicinity of the scaffold position 5 and of the terminal portion of the *n*-pentyl group (R1). Accordingly, in the CoMSIA H-bond donor map (Fig. 8), a cyan area (unfavorable) and a purple region (favorable) are located in the vicinity of the R3 amidic oxygen and nitrogen atoms, respectively. In agreement with these results, **18** [R3 = CONH-(1-adamantyl), pK_i=7.79] results to be more potent than **33** [R3 = NHCO-(1-adamantyl), pK_i=7.59] and **30** [R3 = CH_2NH-(1-adamantyl), pK_i=5.78], and **14** [R3 = CONH-(2-phenylethyl), pK_i=6.70] is more potent than **32** [R3 = NHCO-(2-phenylethyl), pK_i=5.95]. The reliability of the calculations of the H-bond acceptor and donor maps is verified also by the higher affinity of **20** (Y = C, pK_i= 7.80) compared to that of **56** (X = N, pK_i=6.59), and by the higher pK_i values of the R1 *n*-pentyl derivatives **18** (pK_i=7.79) and **20** (pK_i=7.80) in comparison with those of the corresponding R1 *N*-morpholinethyl analogues **25** (pK_i=6.82) and **26** (pK_i=6.66).

Conclusions

The 3D-QSAR studies here presented highlight the key structural features impacting the binding affinity of the 4-oxo-1,4-dihydroquinoline and 4-oxo-1,4-dihydro-1,5-, -1,6- and -1,8-naphthyridine derivatives as selective CB2 agonists. Moreover, allow the prediction of the ligand binding affinity prior to synthesis and they provide useful suggestions for the design of new selective analogues with improved potency.

In fact, taking into account simultaneously all the information deriving from the 3D-QSAR contour maps, we have identified some structural modifications, potentially useful to improve the binding affinity of the series of selective CB2 agonists 4-oxo-1,4-dihydroquinoline and 4-oxo-1,4-dihydro-1,8-naphthyridine derivatives (the 1,5- and 1.6-naphthyridine congeners result to be less promising). In detail, the amidic groups CONH-(3,5-dimethylcyclohexyl), CONH-(4-methylcyclohexyl), CONH-(cycloheptyl), and CONH-(cyclooctyl) would seem particularly favorable as substituent R3. The scaffold position 2 could be unsubstituted or substituted with a fluorine atom. Cyclohexylmethyl, cyclopentylmethyl, 2-cyclobutylethyl, 3-cyclopropylpropyl, *i*-butyl, and pent-1-en-5-yl would result to be effective as substituents R1. A fluorine atom would seem to be optimal as substituent R7, when simultaneously the scaffold position 6 bears a *t*-butyl or a cycloalkyl (cyclopropyl, cyclobutyl, cyclopentyl, cyclohexyl, and cycloheptyl), or a methylene or sulfur atom linked to an *i*-propyl or to the same cycloalkyl groups just mentioned.

Acknowledgments This work was supported by University of Genova. Progetto Ateneo 2007. Fondazione Carige is gratefully acknowledged for financially supporting E.C. and S.C.

References

1. Palmer SL, Thakur GA, Makriyannis A (2002) Cannabinergic ligands. Chem Phys Lipids 121:3–19
2. Howlett AC, Barth F, Bonner TI, Cabral G, Casellas P, Devane WA, Felder CC, Herkenham M, Mackie K, Martin BR, Mechoulam R, Pertwee RG (2002) International union of pharmacology. XXVII. Classification of cannabinoid receptors. Pharmacol Rev 54:161–202
3. Pertwee RG (2001) Cannabinoid receptors and pain. Prog Neurobiol 63:569–611
4. Goya P, Jagerovic N, Hernandez-Folgado L, Martin MI (2003) Cannabinoids and neuropathic pain. Mini Rev Med Chem 3:765–772
5. Calignano A, La Rana G, Piomelli D (2001) Antinociceptive activity of the endogenous fatty acid amide, palmitylethanolamide. Eur J Pharmacol 419:191–198
6. Di Marzo V, Breivogel CS, Tao Q, Bridgen DT, Razdan RK, Zimmer AM, Zimmer A, Martin BR (2000) Levels, metabolism, and pharmacological activity of anandamide in CB(1) cannabinoid receptor knockout mice: evidence for non-CB(1), non-CB(2) receptor-mediated actions of anandamide in mouse brain. J Neurochem 75:2434–2444
7. Hájos N, Ledent C, Freund TF (2001) Novel cannabinoid-sensitive receptor mediates inhibition of glutamatergic synaptic transmission in the hippocampus. Neuroscience 106:1–4
8. Whiteside GT, Lee GP, Valenzano KJ (2007) The role of the cannabinoid CB2 receptor in pain transmission and therapeutic potential of small molecule CB2 receptor agonists. Curr Med Chem 14:917–936
9. Ashton JC (2007) Cannabinoids for the treatment of inflammation. Curr Opin Investig Drugs 2007(8):373–384
10. Giblin GM, O'Shaughnessy CT, Naylor A, Mitchell WL, Eatherton AJ, Slingsby BP, Rawlings DA, Goldsmith P, Brown AJ, Haslam CP, Clayton NM, Wilson AW, Chessell IP, Wittington AR, Green R (2007) Discovery of 2-[(2, 4-dichlorophenyl)amino]-N-[(tetrahydro- 2H-pyran-4-yl)methyl]-4-(trifluoromethyl)- 5-pyrimidinecarboxamide, a selective CB2 receptor agonist for the treatment of inflammatory pain. J Med Chem 50:2597–2600
11. Guindon J, Hohmann AG (2008) Cannabinoid CB2 receptors: a therapeutic target for the treatment of inflammatory and neuropathic pain. Br J Pharmacol 153:319–334
12. Khanolkar AD, Lu D, Ibrahim M, Duclos RI, Thakur GA, Malan TP, Porreca F, Veerappan V, Tian X, George C, Parrish DA, Papahatjis DP, Makriyannis A (2007) Cannabilactones: a novel class of CB2 selective agonists with peripheral analgesic activity. J Med Chem 50:6493–6500
13. Fernandez-Ruiz J, Romero J, Velasco G, Tolon RM, Ramos JA, Guzman M (2007) Trends Pharmacol Sci 28:39–45
14. Maccarrone M, Battista N, Centonze D (2007) The endocannabinoid pathway in Huntington´s disease: a comparison with other neurodegenerative diseases. Prog Neurobiol 81:349–379
15. Centonze D, Finazzi-Agro A, Bernardi G, Maccarrone M (2007) The endocannabinoid system in targeting inflammatory neurodegenerative diseases. Trends Pharmacol Sci 28:180–187

16. McKallip RJ, Lombard C, Fisher M, Martin BR, Ryu S, Grant S, Nagarkatti PS, Nagarkatti M (2002) Targeting CB2 cannabinoid receptors as a novel therapy to treat malignant lymphoblastic disease. Blood 100:627–634
17. Velasco G, Galve-Roperh I, Sánchez C, Blázquez C, Guzmán M (2004) Hypothesis: cannabinoid therapy for the treatment of gliomas? Neuropharmacol 47:315–323
18. Pertwee RG (2002) Cannabinoids and multiple sclerosis. Pharmocol Therapeut 95:165–174
19. Ofek O, Karsak M, Leclerc N, Fogel M, Frenkel B, Wright K, Tam J, Attar-Namdar M, Kram V, Shohami E, Mechoulam R, Zimmer A (2006) Peripheral cannabinoid receptor, CB2, regulates bone mass. Bab I. Proc Nat Acad Sci USA 103:696–701
20. Idris AI, Van't Hof RJ, Greig IR, Ridge SA, Baker D, Ross RA, Ralston SH (2005) Regulation of bone mass, bone loss and osteoclast activity by cannabinoid receptors. Nat Med 11:774–779
21. Lu ZL, Saldanha JW, Hulme EC (2002) Seven-transmembrane receptors: crystals clarify. Trends Pharmacol 23:140–146
22. Pasquini S, Botta L, Semeraro T, Mugnaini C, Ligresti A, Palazzo E, Maione S, Di Marzo V, Corelli F (2008) Investigations on the 4-Quinolone-3-carboxylic acid motif. 2. Synthesis and structure activity relationship of potent and selective cannabinoid-2 receptor agonist endowed with analgesic activity in vivo. J Med Chem 51:5075–5084
23. Manera C, Cascio MG, Benetti V, Allarà M, Tuccinardi T, Martinelli A, Saccomanni G, Vivoli E, Ghelardini C, Di Marzo V, Ferrarini PL (2007) New 1, 8-naphthyridine and quinoline derivatives as CB2 selective agonist. Bioorg Med Chem Lett 17:6505–6510
24. Stern E, Muccioli GG, Bosier B, Hamtiaux L, Millet R, Poupaert JH, Hénichart JP, Depreux P, Goossens JF, Lambert DM (2007) Pharmacomodulations around the 4-oxo-1, 4-dihydroquinoline-3-carboxamides, a class of potent CB2-selective cannabinoid receptor ligands: consequences in receptor affinity and functionality. J Med Chem 50:5471–5484
25. Stern E, Muccioli GG, Millet R, Goossens JF, Farce A, Cravatte P, Poupaert JH, Lambert DM, Depreux P, Hénichart JP (2006) Novel 4-oxo-1, 4-dihydroquinoline-3-carboxamide derivatives as new CB2 cannabinoid receptors agonists: synthesis, pharmacological properties and molecular modeling. J Med Chem 49:70–79
26. MOE: Chemical Computing Group Inc . Montreal. H3A 2R7 Canada. http://www.chemcomp.com
27. Cramer RD III, Patterson DE, Bunce JD (1989) Recent advances in comparative molecular field analysis (CoMFA). Prog Clin Biol Res 291:161–165
28. Klebe G, Abraham U, Mietzner T (1994) Molecular similarity indices in a comparative analysis (CoMSIA) of drug molecules to correlate and predict their biological activity. J Med Chem 37:4130–4146
29. Sybyl 7 0. Tripos Inc 1699 South Hanley Road. St Louis, MO,